Environmental Science & Technology

Article

Cite This: Environ. Sci. Technol. 2019, 53, 651−660

pubs.acs.org/est

Stable Isotope Evidence Shows Re-emission of Elemental Mercury Vapor Occurring after Reductive Loss from Foliage

Wei Yuan,[†,⊥] Jonas Sommar,[*,†] Che-Jen Lin,[†,‡] Xun Wang,[†] Kai Li,[†,⊥] Yi Liu,[†,⊥] Hui Zhang,[†] Zhiyun Lu,[§] Chuansheng Wu,[∥] and Xinbin Feng[*,†]

[†]State Key Laboratory of Environmental Geochemistry, Institute of Geochemistry, Chinese Academy of Sciences, Guiyang 550081, China

[‡]Center for Advances in Water and Air Quality, Lamar University, Beaumont, Texas 77710, United States

[§]Key Laboratory of Tropical Forest Ecology, Xishuangbanna Tropical Botanical Garden, Chinese Academy of Sciences, Mengla 666303, China

[∥]Anhui Province Key Laboratory of Environmental Hormone and Reproduction, Fuyang Normal University, Anhui 236037, China

[⊥]University of Chinese Academy of Sciences, Beijing 100049, China

Supporting Information

ABSTRACT: The mechanism of elemental mercury (Hg^0) re-emission from vegetation to the atmosphere is currently poorly understood. In this study, we investigated branch-level Hg^0 atmosphere-foliage exchange in a pristine evergreen forest by systematically combining Hg isotopic composition, air concentration and flux measurements to unravel process information. It is found that the foliage represents a diurnally changing sink for atmospheric Hg^0 and its Hg content increases with leaf age and mass. Atmospheric Hg^0 is the dominant source of foliar Hg and the involvement of Hg^{II} is not supported by isotopic evidence. Upon Hg^0 uptake, maturing foliage becomes progressively enriched in lighter Hg isotopes and depleted in odd mass isotopes. The measured isotopic composition of foliage Hg and isotopic shift caused by Hg^0 evasion from foliage supports that Hg^0 emitted from foliage is derived from Hg previously metabolized and bound in the leaf interior then subsequently recycled after reduction, and not merely a retroflux of recently deposited Hg^0 on foliar surface. An isotopic differential mass balance model indicates that the proportion of foliar Hg^0 efflux to uptake gradually increase from emergence to senescence with an average flux ratio of 30%.

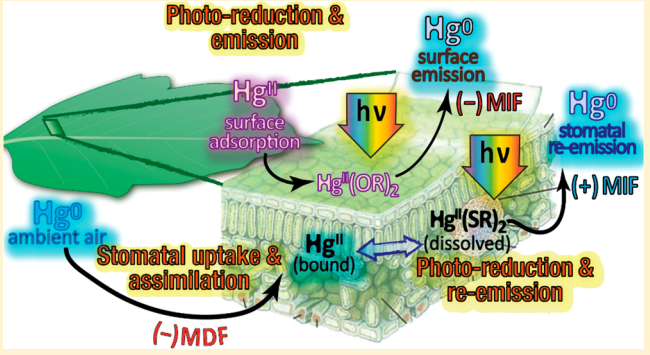

1. INTRODUCTION

Mercury (Hg) is a persistent pollutant that causes health and ecological concerns globally. Gaseous elemental mercury (Hg^0), the primary form of Hg in the atmosphere, goes through deposition and re-emission cycles after it is released and is transformed in multiple environmental compartments.[1] Globally, forest ecosystems emerge as a net sink of atmospheric Hg^0 which may divert nearly ∼20% of its total burden (5000 Mg) annually.[2,3] Nonetheless, a lack of understanding in spatial and temporal forest-soil-atmosphere Hg^0 exchange causes large uncertainties for constraining Hg^0 exchange over natural surfaces globally.[4,5] There remain considerable unknowns in the sources and sinks of Hg^0 in forest vegetation, the extent of partial re-emission back to the atmosphere and its governing processes, and the effect of environmental controls on the magnitude and dynamics of Hg^0 fluxes.[6−10]

Previous investigations using enriched isotopic spikes and nonisotopic, total Hg measurements mainly focus on the quantification of air−foliage exchanges.[6] These studies have limitation in separating the evasion and deposition fluxes. Recent advancements in stable Hg isotope techniques reveal that Hg translocation and transformation processes in forest ecosystems produce specific signals of mass-dependent fractionation [MDF, reported as δ^{202}Hg] and mass-independent fractionation [MIF, reported as $\Delta^{199}Hg/\Delta^{200}Hg/\Delta^{201}Hg$].[11−14] It has been suggested that dry deposition of Hg^0 to pristine biomes accounts for a substantial portion of atmospheric Hg deposition.[15−18] Although isotopic data on bulk foliage and ambient air have been recently reported,[8,12,13,16,19] information on the dynamic Hg^0 flux components is largely unknown, in addition to the lack of understanding on the progression of Hg isotope ratios in forest foliage from emergence to senescence. It has been suggested that re-emission of Hg^0 from foliage is triggered by continuously photoreduction of Hg^{II} previously retained by

Received: August 30, 2018
Revised: November 20, 2018
Accepted: December 3, 2018
Published: December 3, 2018

DOI: 10.1021/acs.est.8b04865
Environ. Sci. Technol. 2019, 53, 651−660

Table 1. Summary of Air–Leaf Hg^0 Fluxes Measured by the DFB Technique (Including Data within ± σ of the Measured DFB Blank, % of (Significant) Flux Data Outside This Interval Is Listed below) with Data Deriving from Washed Foliage within Parentheses, Ambient Air Hg^0 Concentrations and Auxiliary Meteorological and Environmental Observations (Presented as 40 min Averages) during the Eight Campaigns for Each of the Species LX, CW, and SN

species	variable	ambient #1	ambient #2 (dark)	ambient #3	ambient #4 (dark)	ambient #5	zero #1	zero #2	zero #3
Lithocarpus xylocarpus	date	7–10 April, 2016	11–14 April, 2016	25–28 Sept. 2016	29 Sept. – 2 Oct. 2016	26–31 Dec., 2016	3–7 April, 2016	1–5 July, 2016	26–30 July, 2016
	Hg^0 flux (ng m^{-2} h^{-1})	0.53 ± 0.24 (0.30 ± 0.16)	0.13 ± 0.17 (0.04 ± 0.13)	−0.41 ± 0.28 (−0.36 ± 0.18)	−0.63 ± 0.27 (−0.86 ± 0.27)	−0.16 ± 0.10 (−0.39 ± 0.23)[a]	0.91 ± 0.43 (0.41 ± 0.18)	0.27 ± 0.12 (0.15 ± 0.05)	0.22 ± 0.12 (0.20 ± 0.11)
	Leaf concentrations (ng g^{-1})[b]	6.3 ± 1.7	6.3 ± 1.7	19.9 ± 6.2	19.9 ± 6.2	42.6	6.3 ± 1.7	10.3 ± 0.2	13.4 ± 0.2
	% flux data > blank[c]	52 (39)	22 (14)	94 (95)	100 (100)	87 (95)	62 (50)	100 (100)	99 (97)
	Air Hg^0 conc. (ng m^{-3})	1.59 ± 0.06	1.66 ± 0.08	1.81 ± 0.31	1.89 ± 0.57	1.64 ± 0.21	0.01 ± 0.01	0.002 ± 0.004	0.002 ± 0.005
	Leaf area (m^2)	0.124(0.225)	0.124(0.225)	0.353(0.372)	0.353(0.372)	0.394(0.391)	0.124(0.225)	0.358(0.542)	0.530(0.435)
	PAR photon flux (μE m^{-2} s^{-1})	126.7 ± 202.7		29.9 ± 41.2		24.5 ± 37.4	97.8 ± 153.7	25.9 ± 32.2	43.8 ± 66.3
	air temperature (°C)	14.3 ± 1.9	14.7 ± 2.2	15.6 ± 2.0	14.6 ± 2.9	6.6 ± 1.4	12.0 ± 1.5	15.2 ± 0.7	15.1 ± 1.6
	air humidity (%)	35.0 ± 5.9	52.0 ± 10.9	91.7 ± 7.8	91. Two ±9.2	90.1 ± 8.3	76.7 ± 9.4	98.5 ± 2.5	90.9 ± 6.8
Castanopsis watii	date	23–27 March, 2016	30–31 March, 2016	16–19 Sept., 2016	20–23 Sept. 2016	21–25 Dec., 2016	17–20 March, 2016	24–28 June, 2016	19–23 July, 2016
	Hg^0 flux (ng m^{-2} h^{-1})	−0.57 ± 0.81 (0.13 ± 0.44)	−0.37 ± 0.16 (−0.19 ± 0.21)	−0.94 ± 0.13 (−0.33 ± 0.29)	−2.57 ± 0.24 (−1.46 ± 0.26)	−0.68 ± 0.08 (−0.95 ± 0.11)[a]	0.60 ± 0.76 (0.49 ± 0.63)	0.16 ± 0.09 (0.15 ± 0.09)	0.11 ± 0.03 (0.06 ± 0.02)
	leaf concentrations (ng g^{-1})[3]	6.5 ± 0.7	6.5 ± 0.7	39.1 ± 8.9	39.1 ± 8.9	64.2	6.5 ± 0.7	21.1 ± 2.9	33.5 ± 8.5
	% flux data > blank[2]	100 (100)	100 (100)	100 (92)	100 (100)	100 (99)	46 (39)	100 (100)	100 (53)
	air Hg^0 conc. (ng m^{-3})	3.86 ± 1.41	1.52 ± 0.05	1.46 ± 0.15	3.32 ± 0.20	1.27 ± 0.07	0.01 ± 0.03	0.005 ± 0.006	0.000 ± 0.005
	leaf area (m^2)	0.274(0.299)	0.274(0.299)	0.563(0.403)	0.563(0.403)	0.309(0.421)	0.274(0.299)	0.916(0.509)	0.435(0.482)
	PAR photon flux (μE m^{-2} s^{-1})	115.0 ± 174.5		22.9 ± 31.5		20.3 ± 30.8	115.3 ± 198.7	46.5 ± 69.1	16.0 ± 18.8
	air temperature (°C)	9.8 ± 3.1	12.6 ± 2.5	14.6 ± 1.5	11.8 ± 1.1	7.6 ± 1.0	10.9 ± 2.4	16.0 ± 1.4	13.7 ± 0.6
	air humidity (%)	71.4 ± 16.3	62.1 ± 11.2	91.9 ± 9.0	97.1 ± 3.7	88.7 ± 5.3	49.7 ± 10.3	95.8 ± 6.1	
Schima noronhae	date	19–22 April 2016	25–28 April 2016	5–9 Sept., 2016	12–15 Sept. 2016	1–4 Jan., 2017	14–18 April, 2016	19–23 June, 2016	7–10 July, 2016
	Hg^0 flux (ng m^{-2} h^{-1})	−0.16 ± 0.04 (−0.12 ± 0.07)	−0.04 ± 0.05 (−0.06 ± 0.04)	−1.60 ± 0.41 (−0.70 ± 0.33)	−0.65 ± 0.35 (−0.27 ± 0.18)	−0.60 ± 0.17 (−0.84 ± 0.24)[a]	0.25 ± 0.10 (0.19 ± 0.07)	0.12 ± 0.04 (0.07 ± 0.02)	0.22 ± 0.19 (0.14 ± 0.10)
	leaf concentrations (ng g^{-1})[b]	6.6 ± 0.6	6.6 ± 0.6	23.2 ± 5.2	23.2 ± 5.2	52.1	6.6 ± 0.6	11.6 ± 4.2	14.3 ± 1.6
	% flux data > blank[c]	73 (68)	100 (100)	100 (100)	95 (92)	97 (98)	90 (48)	100 (100)	100 (100)
	air Hg^0 conc. (ng m^{-3})	1.63 ± 0.07	1.51 ± 0.08	1.63 ± 0.21	2.11 ± 0.31	1.34 ± 0.20	0.01 ± 0.01	0.002 ± 0.004	0.002 ± 0.005
	leaf area (m^2)	0.290(0.331)	0.290(0.331)	0.363(0.565)	0.363(0.565)	0.321(0.555)	0.290(0.331)	0.589(0.980)	0.523(0.681)
	PAR photon flux (μE m^{-2} s^{-1})	86.2 ± 119.6		20.4 ± 26.6		17.5 ± 26.7	86.2 ± 119.6	18.8 ± 23.1	44.0 ± 83.1
	air temperature (°C)	11.8 ± 1.5	13.1 ± 2.4	15.1 ± 0.9	14.2 ± 2.1	6.6 ± 0.9	11.8 ± 1.5	14.2 ± 0.6	15.8 ± 1.7
	air humidity (%)	72.6 ± 4.6	68.8 ± 10.7	98.6 ± 1.9	91.8 ± 7.8	95.1 ± 4.5	72.6 ± 4.6		

[a]Refer to dark and not to wash treatment. [b]The accurate sampling time is shown in the Table S11. [c]$|C_{out}-C_{in}|$ > 0.027 ng m^{-3} (1σ of the measured DFB blank).

DOI: 10.1021/acs.est.8b04865
Environ. Sci. Technol. 2019, 53, 651–660

leaf,[16,17,19] since substantial odd-MIF signatures are primarily of photochemical origin.[20] However, little is known about the isotopic shift caused by the re-emission of Hg previously deposited on natural surfaces.

The objective of this study is to isotopically examine foliar air−surface exchange under ambient air and Hg-free air exposures to understand the process of Hg^0 uptake and re-emission by forest vegetation. Concurrent, temporally resolved measurements of Hg^0 concentration and foliage−atmosphere Hg^0 exchange in a pristine evergreen forest were conducted to discern the progression of Hg content and isotopic composition in leaf from emergence to senescence caused by the uptake and re-emission cycle. Selected experiments were also performed to understand the forms of atmospheric Hg deposited on foliage and the role of natural light in facilitating the re-emission process. An isotope mixing model was constructed to understand the impact of the foliage uptake of elemental Hg vapor on the lifetime and isotopic shift of atmospheric Hg at a global scale.

2. METHODS

2.1. Site Description. The study site is located within the experimental area of the Ailaoshan Station for Subtropical Forest Ecosystem Research Studies (ASSFERS, 24°32′N, 101°01′E, 2476 m elevation), Yunnan province, China. The site description has been discussed in detail in Section S1 of the Supporting Information (SI). Briefly, the canopy level is dominated by old-growth (stand age >300 yr) and evergreen beech species (canopy coverage ≥85%), such as *Lithocarpus chintungensis*, *Lithocarpus xylocarpus* (LX), and *Castanopsis wattii* (CW). *Schima noronhae* (SN), *Rhododendron leptothrium*, and *Manglietia insignsis* in the subcanopy. Our study focused on the foliage of the three dominant species LX, CW, and SN, which cumulatively account for ∼55% of the tree density (2728 stems ha^{-1}).

2.2. Hg^0 Concentration and Flux Measurement. The progression of foliar Hg^0 uptake and gas exchange over the growing season was examined through field measurement incorporating branch enclosures[6−10] with analysis of regularly harvested plant leaves. Although the enclosure flux method has inherited limitations such as induced greenhouse effects and isolation from ambient air, it is regarded as one the most versatile approaches to quantify the air−surface exchange of Hg^0 vapor due to its reliability, field applicability and its versatility for investigating environmental factors.[4,21,22]

Branch-level foliar air−surface Hg^0 exchange measurements were conducted using two Tedlar dynamic flux bags (DFBs) coupled with an automated Hg vapor analyzer (Model 2537X, Tekran Instruments Corp., Canada) via a synchronized four-port sampling system (Tekran Model 1115) for sequential Hg analysis of air entering and exiting each of the DFBs. A detailed scheme of the experimental setup (Figure S1), a comprehensive description of the operating procedure, calculation of Hg^0 fluxes, sampling of Hg^0 vapor for subsequent measurements of mercury isotope, as well as the calibration of instrument and measures of quality control are presented in Section S2 of the SI. The bidirectional air−foliage exchange fluxes were measured over the three predominating tree species. Hg^0 vapor in the air near the inlet and from the outlet of the DFBs was also sampled using chlorine-impregnated activated carbon (ClC) traps[23] for determination of stable Hg isotopes. Each ClC-trap sample represents an integrated signal for both daytime and nighttime processes during each experimental cycle (∼4 days). The air Hg^0 concentration and Hg mass sampled in each ClC trap are shown in Tables S5−S8. The mean capture efficiency of atmospheric Hg^0 by ClC traps was 100.1 ± 10.4% (±1σ, n = 62).

2.3. Foliage Sample Collection and Preparation. Following an experiment, the enclosed foliage was harvested to determine the single-sided projected leaf area using a calibrated computer scanner and digital image processing software (NIH, U.S.A.). Independently, current-year leaves of the investigated species were collected in the community at approximately 10 m above ground level (∼40% of the average canopy height) every month during March 2016 to March 2017 (∼10 to >360 days age). The leaf area of each collection batch was determined as aforementioned. Subsequently, the leaves were air-dried and ground to a fine powder by a precleaned blender. A portion of the sample was analyzed for total Hg content by a Lumex RA-915 analyzer (Lumex Ltd., Russia) equipped with a pyrolysis attachment (detection limit: 1 ng g^{-1}).[24] The method recovery was 97.6 ± 6.1% (n = 4) using a BCR certified reference material (BCR-482, 480 ± 20 ng g^{-1}) and the uncertainty for all samples of replicates is <5%.

2.4. Stable Hg Isotope Measurement. The exposed ClC traps (for ambient air and DFB outlet air with a Hg^0 mass load >10 ng) and foliage samples were processed using a double-stage offline combustion-trapping technique[25] to preconcentrate the captured Hg into 5-mL oxidizing trapping solution of 40% mixture of nitric and hydrochloric acid ("reverse aqua regia", HNO_3:HCl = 2:1, v/v). The Hg isotope composition were measured by MC-ICP-MS using a Nu II Plasma mass spectrometer (Nu Instruments, U.K.). A detailed scheme of the experimental setup, a comprehensive description of the operating procedure, and reproducibility of isotope measurements can be found in Section S3 of the SI. Following Blum and Bergquist,[11] MDF is reported as $\delta^{202}Hg$ (‰) = 1000 × $[(^{202}Hg/^{198}Hg)_{sample}/(^{202}Hg/^{198}Hg)_{NIST3133} - 1]$ and MIF is calculated as $\Delta^{xxx}Hg = \delta^{xxx}Hg - \delta^{202}Hg \times \beta_{xxx}$, where β_{xxx} is 0.252 for ^{199}Hg, 0.502 for ^{200}Hg, and 0.752 for ^{201}Hg, respectively.

2.5. Quality Assurance and Control. Figure S2 shows the effects of chamber heating and wall condensation during the measurement. Briefly, the temperature and RH inside the flux bag was 0.6 ± 1.8 °C higher and 3.1 ± 6.1% lower than the values outside, respectively, indicating a mild greenhouse effect on the foliage under the high purging flow. After each experiment, there was no visual difference between enclosed and unenclosed plant materials. In addition, the measured fluxes are statistically different from the chamber blanks (average 0.009 ± 0.027 ng m^{-3}, n = 72, Figure S3). Furthermore, measurements made with empty flux bags show Hg isotopic composition of ambient air samples at the inlet were essentially identical to the values found at the outlet (differences between the two ports: $\delta^{202}Hg$:0.03 ± 0.05‰, $\Delta^{199}Hg$:0.00 ± 0.02‰, $\Delta^{200}Hg$:0.02 ± 0.00‰, $\Delta^{201}Hg$: −0.01 ± 0.01‰, n = 3, ± 1σ, Table S1). On the basis of the data, the influences caused by system artifacts (e.g., sorption−desorption, chamber heating and wall condensation) on the measured fluxes and isotopic compositions are negligible given the experimental conditions. The enclosed leaf area ranges from 0.124 to 0.565 m^2 (0.36 m^2 on average) during the entire experiments (details shown in Table 1). The difference of Hg concentration between the inlet and outlet air ranges from −2.2 to 0.3 ng m^{-3} (mean: −0.29 ng m^{-3}, Figure S3). Such difference was up to 20 times higher than the lower measured

DOI: 10.1021/acs.est.8b04865
Environ. Sci. Technol. 2019, 53, 651−660

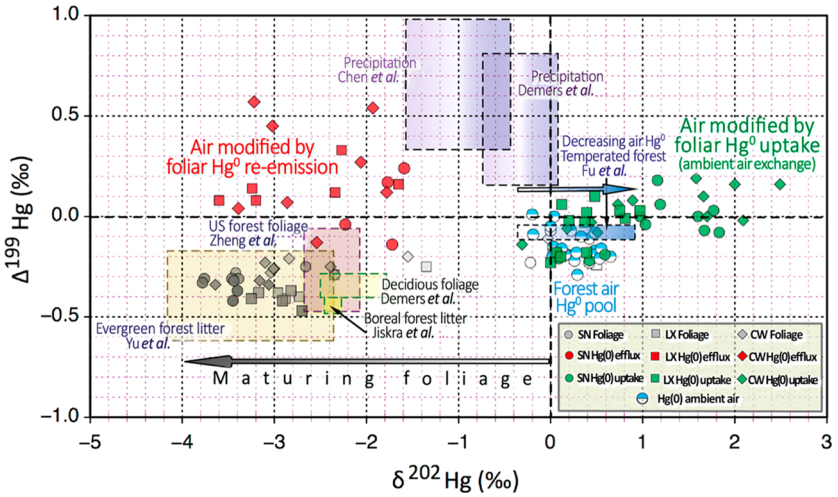

Figure 1. Observed Hg isotope composition in various aerial and aerial-influenced compartments of the ASSFERS forest ecosystem. Inlaid rectangles represent isotopic ranges reported in selected previous relevant studies which contain atmospheric Hg isotopic composition data from Fu et al.,[8] open field precipitation Hg isotopic composition data from Demers et al.,[16] and Chen et al.[40] and foliar Hg isotopic composition data from Demers et al.,[16] Jiskra et al.,[14] Yu et al.,[19] and Zheng et al.[17] The filled arrows associated with "Maturing Foliage" and "Decreasing air Hg^0" indicate the direction of $\delta^{202}Hg^{II}$ (leaf) during foliage growing and $\delta^{202}Hg^0$ in forest air during foliage Hg^0 uptake process, respectively. The points marked "Air modified by foliar Hg^0 re-emission" in red and "Air modified by foliar Hg^0 uptake" in green are the efflux observed using Hg-free inlet air and ambient air inlet, respectively.

limits of Tekran 2537X (0.1 ng m^{-3}). Given the −1 to −3 ‰ shift of $\delta^{202}Hg$ during Hg^0 uptake by foliage and distinct Hg^0 uptake in flux bag, the signals of air−foliage flux and shifts of Hg isotopic compositions can confidently detected.

3. RESULTS AND DISCUSSION

3.1. Air−Leaf Hg^0 Exchanges under Ambient and Treatment Conditions. Eight Hg^0 flux measurement campaigns were conducted for each of species *Lithocarpus Xylocarpus* (LX), *Castanopsis Wattii* (CW) and *Schima Noronhae* (SN) from March 2016 to January 2017. Three experiments were conducted using Hg free air for observing Hg^0 re-emission from foliage. The other five campaigns observed the flux behavior under ambient air exposure. The experiments in two out of the five campaigns were performed by blocking the light from the foliage (dark treatment). The net Hg^0 flux was negative in all but two campaigns (Table 1), indicating Hg^0 uptake by leaves. Different flux values were observed for the species investigated. Cumulative foliar uptake decreases in the order CW > SN > LX (Table 1).

Air−foliage Hg^0 exchange is controlled by many factors, such as the meteorological conditions (light, temperature, humidity, etc.), air Hg^0 concentration (Figure S4), and vegetation species.[9,26,27] The observed Hg^0 fluxes in individual campaigns exhibited significant ($p < 0.001$, 2-tailed t test) positive correlations with PAR ($0.45 \leq r \leq 0.95$) and air temperature ($0.33 \leq r \leq 0.82$), and anticorrelations with air humidity ($-0.88 \leq r \leq -0.21$) and air Hg^0 concentration ($-0.61 \leq r \leq -0.18$).

Air−surface exchange of Hg^0 is bidirectional with alternating periods of emission and deposition being commonly observed during a day.[28−30] The diurnal features shown in this study are based on the mean values measured in the sampling period and shown each subplot. The observed fluxes show small deposition at night and gradually shift to evasion at mid-day, then to deposition again in early evening (Figures S5−S7). The dark treatment (Table 1 [#2 and #4], and Table S3) diminishes the mid-day evasion originally observed under sunlight (significantly lower, $p < 0.001$, t test), suggesting that the transient evasion is induced by light.[6,10]

The study site locates in subtropical evergreen forest regions, and has distinct dry (November to May) and rainy seasons.[2] The warmer and wetter climate in the rainy season leads to rapid vegetation growth. Not surprisingly, the net flux in the rainy season (mean flux is -0.41 ± 0.28, -0.94 ± 0.13, and -1.60 ± 0.41 ng m^{-2} h^{-1} for LX, CW, and SN, respectively) is much more negative than the flux in the dry season (mean flux is 0.19 ± 0.34, -0.63 ± 0.89, and -0.38 ± 0.21 ng m^{-2} h^{-1} for LX, CW and SN, respectively). The stronger observed Hg^0 sink caused by foliage uptake in rainy season is consistent with earlier studies. Earlier long-term whole-ecosystem Hg^0 fluxes studies reveal growing-seasonal trends of the flux direction and magnitude that are influenced by environmental and biological factors.[29−32]

Experiments performed under controlled environment conditions provide process insights for air−foliage Hg^0 exchange.[33−35] Consistent Hg^0 re-emission from foliage is observed with Hg-free air as the purging gas (Figures S8−S10). The variation of such Hg^0 re-emission is influenced by PAR. Peak fluxes were observed for all species in early afternoon (12−14 h) in good correlations with PAR ($0.79 \leq r \leq 0.97$, Table S4). The most positive fluxes were found in the dry season (Table 1) during which the magnitude of Hg^0 evasion followed the order LX ≃ CW (~2.5 ng m^{-2} h^{-1}) ≫ SN (~0.7 ng m^{-2} h^{-1}). During the moist June and July with diminished PAR levels, foliar Hg^0 efflux from LX and CW was reduced to less than one-third of the original flux; while the flux for SN was moderately decreased.

A significant difference was found in Hg^0 re-emission using Hg^0-free air between the untreated and treated (washed) enclosed branches. The untreated group has approximately 30% greater fluxes compared to the treated group (Table 1). Presumably, the lowered net emission flux from washed leaves is presumably derived from the removal of deposited Hg^{II} species (particulate matters deposited on leaves prior to experiments) that otherwise may gradually undergo reduction

DOI: 10.1021/acs.est.8b04865
Environ. Sci. Technol. 2019, 53, 651−660

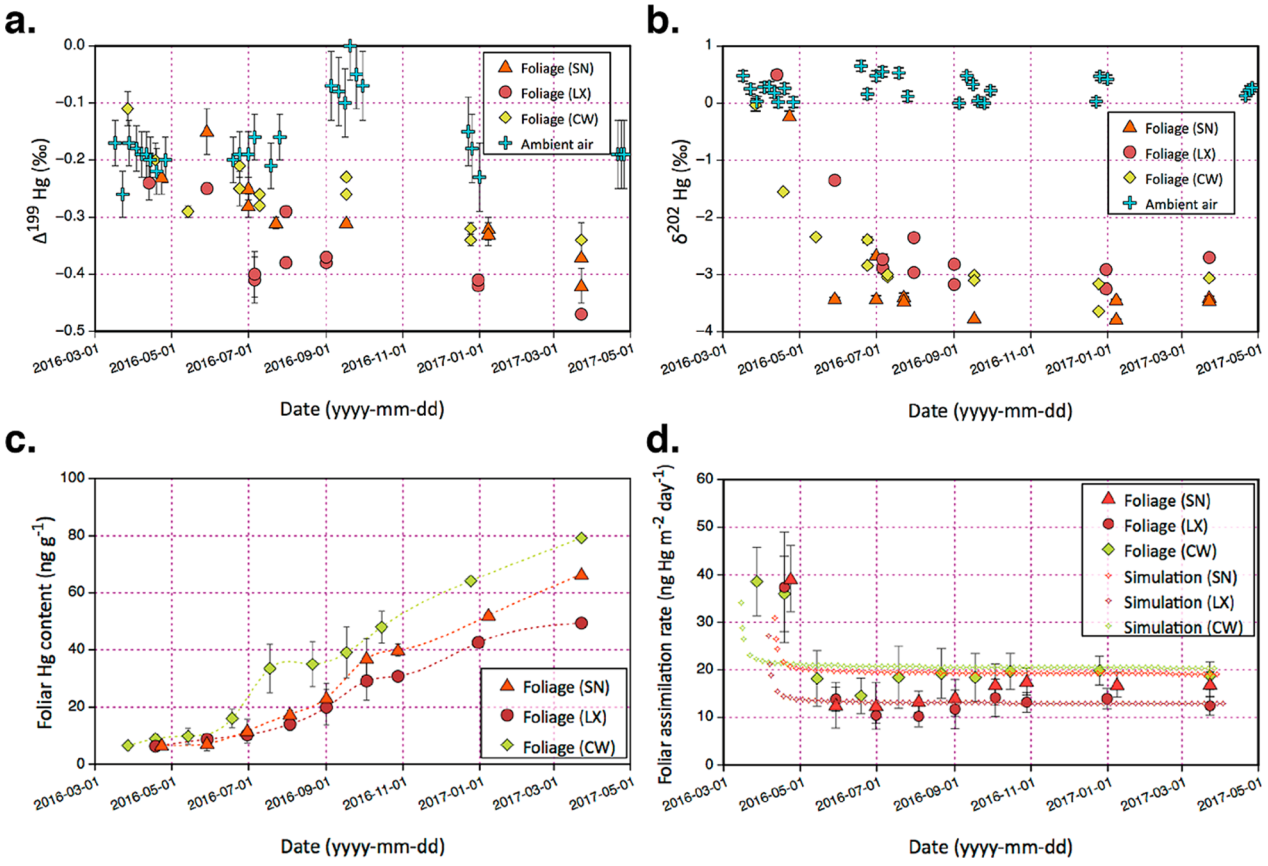

Figure 2. Mercury isotopic variation (a: Δ^{199}Hg and b: δ^{202}Hg), mercury content (c) and assimilation rate (d) variation in leaves during foliage maturation. The error bars indicate ±2 and ±1 standard deviation for a and b and c and d, respectively. Simulated assimilation rates (SI Section S4) are inlaid in Panel 2d.

and subsequent Hg^0 evasion. Another possible reason is that the leaf washing may change surface chemical properties, such as removal of waxes and associated sorption sites, which can possibly modify the uptake and re-emission processes.[36,37]

3.2. Hg Isotopic Signatures in Air, Foliage and Flux Components. It has been shown that Hg stored in foliage is derived primarily from atmospheric Hg^0 uptake.[15−17] Lighter Hg isotopes in air are preferentially accumulated in the foliage, causing a −3.0‰ to −1.0‰ δ^{202}Hg shift (MDF) between air and foliage.[12,20,38] Re-emission of Hg^0 also tends to release lighter Hg isotopes. Atmospheric Hg^0 oxidation has been proposed as the main cause for even-MIF[20,39] based on the distinct Δ^{200}Hg signatures (range: 0.08−1.18‰, mean: 0.25 ± 0.19‰, n = 47, ± σ) observed in precipitation at remote sites (p < 0.05, by one sample t test), while most other environmental samples showed ∼0 Δ^{200}Hg.[16,40−42] The odd-MIF is primarily explained by two mechanisms: magnetic isotope effect (MIE)[43] and nuclear volume effect (NVE).[44] The odd-MIF fractionation departs during Hg^{II} photoreduction (MIE) depending on electron donor ligands that form complexes with Hg^{II} [45]. Positive (+) odd-MIF is typically found in the re-emitted Hg^0 from the reduction of Hg complexes containing reduced sulfur functional groups (e.g., Hg-SR), while Hg^{II} photoreduction in an oxygen-donor environment typically yields (−) odd-MIF.[16]

In this study, Hg isotopic composition differs substantially between investigated reservoirs and fluxes within the forested ecosystem as showed in the triple signature (δ^{202}Hg−Δ^{199}Hg−Δ^{200}Hg). Air from the DFB inlet or outlet position and foliage of various ages shows insignificant values oscillating near zero in Δ^{200}Hg (Tables S5−S10). In the Δ^{199}Hg−δ^{202}Hg space, Figure 1 depicts the characteristics of ambient air Hg^0 samples collected at the forest site for the whole year ($\delta^{202}Hg^0$ = 0.26 ± 0.39‰, $\Delta^{199}Hg^0$ = −0.16 ± 0.12‰, n = 27) and the isotopic data ranges for relevant pools reported in previous forest studies.[8,14,16,17,19] This isotope signature of Hg^0 overlaps with observations made in China[8,19] and U.S. forests[16] (all p > 0.05, One-Way ANOVA).

Examination of the isotope composition of juvenile leaves (10−15 days old sprouts with a total Hg content of 6.4 ± 0.8 ng g^{-1} representing pooled samples from several trees of each species; LX: $\delta^{202}Hg^{II}$ = 0.50 ± 0.09‰, $\Delta^{199}Hg^{II}$ = −0.24 ± 0.04‰; CW: $\delta^{202}Hg^{II}$ = −0.03 ± 0.11‰, $\Delta^{199}Hg^{II}$ = −0.11 ± 0.04‰; SN: $\delta^{202}Hg^{II}$ = −0.22 ± 0.09‰, $\Delta^{199}Hg^{II}$ = −0.23 ± 0.04‰) shows unanimously characteristic of ambient air Hg^0 but differs substantially from that of open field precipitation with positive $\Delta^{199}Hg^{II}$ (Figure 1), implying that foliar Hg uptake derives from stomatal uptake of Hg^0.

In contrast to the Hg pool in sprouts, Hg in current-year growing foliage shifts during the initial months rapidly toward distinctly negative δ^{202}Hg-signatures (Figures 1 and 2b). Concurrently, a slower progression toward negative odd-MIF is apparent (Figure 2a). After approximately 2−4 months of age depending on species, the leaf MDF decline levels off at an average 2.7−3.1‰ lower δ^{202}Hg than that of ambient Hg^0. Such trend can be attributed to several causes. One is that the Hg concentration in the leaves is rising (Figure 2c) and the assimilation rate is decreasing (Figure 2d). Such a trend of

DOI: 10.1021/acs.est.8b04865
Environ. Sci. Technol. 2019, 53, 651−660

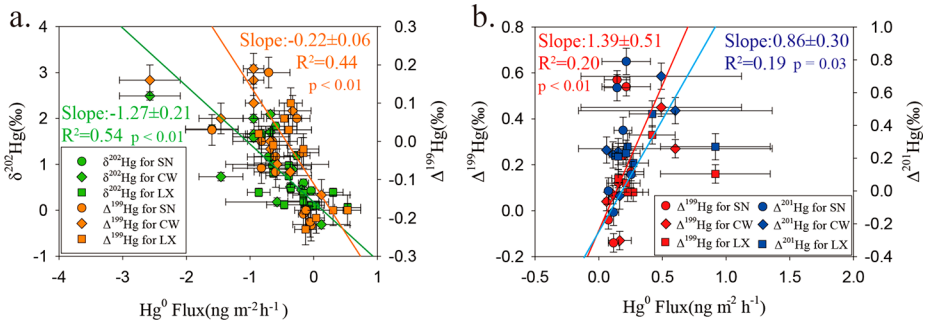

Figure 3. Scatterplot of δ^{202}Hg and Δ^{199}Hg signatures versus Hg^0 flux from all DFB experiments using ambient air purging (a) and scatterplot of Δ^{199}Hg and Δ^{201}Hg signatures versus Hg^0 flux from all DFB experiments using Hg free air purging (b). The error bars represent ±2 standard deviation. The lines represent Williamson-York bivariate regression fitting. Each slope is given with one standard error of the mean and below the square of Pearson correlation coefficient (R^2) and *p*-value (two-tailed *t* test) are added.

assimilation rate means the fraction involved in the reaction is decreasing, leading to a swiftly decreasing fraction and increasing MDF. Another possibility is that additional Hg uptake is "diluted" by existing Hg accumulated in foliage, thus a slower change in the fractionation of $^{202}Hg^{II}$. Furthermore, as the foliage matures, the gradually increased Hg re-emission sends (−)MDF back to ambient air and induces a (+)MDF in foliage, which is supported by the experiments conducted using Hg-free air. The reemission process can partly offset the (−)MDF caused by foliage uptake. Nevertheless, all species displayed a continued foliar Hg assimilation through the growing season (Figure 2c and Table S11). In contrast to MDF shift, there is a continually augmented negative shift in odd-MIF (Figure 2a). This can be explained by the different mechanisms causing MDF and MIF during foliage growth since MIF is merely triggered by photo reduction followed by Hg^0 re-emission. The oldest leaves (~1-year age) before senescence exceed the total Hg content of 50−80 ng g^{-1} (dry weight basis) and display Δ^{199}Hg from −0.47 to −0.34‰ depending on species.

As a composite, the isotopic signature of the air samples from the DFB outlet (corresponding to $-2.57 \leq FHg^0 \leq 0.53$ ng m^{-2} h^{-1}, $n = 36$) during ambient air exposure of foliage represents a range ($\delta^{202}Hg^0 = 0.86 \pm 0.74$‰, $\Delta^{199}Hg^0 = -0.03 \pm 0.12$‰) complementary to that of maturing foliage in the δ^{202}Hg−Δ^{199}Hg space (Figure 1). Moreover, the enrichment of heavier isotopes ($\delta^{202}Hg^0$ up to 2.49‰) in the outlet air (generally deficits in Hg^0) displays a significant negative correlation ($p < 0.001$, two tailed *t* test) with the Hg^0 deposition flux. The associated Williamson-York bivariate regression fit in Figure 3a shows that the magnitude of MDF of Hg^0 in exchanged ambient air decreases with weaker net fluxes. The MDF level increases in the order LX ($\delta^{202}Hg^0 = 0.33 \pm 0.08$‰, $n = 12$) < SN ($\delta^{202}Hg^0 = 0.93 \pm 0.38$‰, $n = 12$) < CW ($\delta^{202}Hg^0 = 0.96 \pm 0.64$‰, $n = 12$), following the order of cumulative foliar uptake observed. The Hg^0 efflux under Hg-free air displays δ^{202}Hg at −2.47 ± 0.68‰ ($n = 18$), slightly more negative than that of foliage but not significant (an average of −0.15‰ shift, $p = 0.69$, by two-tailed independent samples test, Tables S6, S7, and S10). This shift is most likely caused by the dilution of the re-emission induced (+) MDF signal by the Hg stored in foliage, or by secondary transformation in foliage (e.g., Hg adsorption−desorption in leaf interior), and then offsetted by (−) MDF during Hg^0 uptake process.

However, there is a significant anticorrelation between odd-MIF ($\Delta^{199}Hg^0$ in Figure 3a) and FHg^0, revealing the role of foliage as a bidirectional exchange surface where Hg^0 uptake and re-emission take place simultaneously (i.e., Hg^0 uptake rate positively correlates with the Hg^0 re-emission rate). The magnitude and range (~0.4‰) of Δ^{199}Hg-values observed in ambient air exchange did not approach the positive odd-MIF observed in the unidirectional Hg^0 flux using Hg free air as the purging gas. Interestingly, the isotopic identity (in terms of positions in the Δ^{199}Hg−δ^{202}Hg space) of the efflux observed using Hg-free inlet air (i.e., air modified by foliar Hg^0 re-emission in Figure 1) is distinct from the signatures observed under ambient air (i.e., air modified by foliar Hg^0 uptake in Figure 1). The efflux samples have positive odd-MIF signatures ($\Delta^{199}Hg = 0.17 \pm 0.20$‰; $\Delta^{201}Hg = 0.29 \pm 0.25$‰) in contrast to ambient air and leaf samples. Such (+) odd-MIF in Hg^0 re-emissions is consistent with Hg complexes formed with reduced sulfur functional groups (e.g., Hg-SR).[16]

Associated with Hg-free air supply, FHg^0 in the range 0.06−0.91 ng m^{-2} h^{-1} is insignificantly correlated with δ^{202}Hg ($p = 0.21$, two-tailed test in correlation analysis) but displays larger correlations with odd-MIF (Δ^{199}Hg and Δ^{201}Hg, $p = 0.01$ and 0.03, two-tailed test in correlation analysis, Figure 3b). Meanwhile, we also found that such odd-MIF is also positively correlated to PAR ($R^2 = 0.63$, $p < 0.01$, two-tailed test in correlation analysis, Figure S11). These correlations suggest that the increased intensity of PAR induces greater Hg^0 release and the continuous photoreduction gradually increases the magnitude of MIF signatures in the smaller Hg pool remaining in the stomatal cavities. Meanwhile, there is a strong negative correlation between odd-MIF versus leaf area (Figure S12). Such a correlation indicates that a larger leaf area facilitates stronger photoreduction and promotes re-emissions, driving a more negative odd-MIF signature in leaf samples. The stronger photoreduction also imposes a greater influence on leaves containing smaller foliar Hg mass in same area.

This isotopic evidence supports that Hg^0 emitted from foliage is predominantly derived from Hg previously metabolized (oxidized), bound in the leaf interior and then subsequently recycled upon reduction, instead of merely a retroflux of recently air-exchanged Hg^0 by the foliar gas−air interface. This is supported by several observations. First, the Hg isotopic signatures of efflux samples under Hg-free air differ from the signatures of ambient air samples. Specifically, the large shift in $\Delta^{199}Hg^0$ of +0.45‰ compared to ambient air Hg^0 suggests photoreduction and then Hg^0 re-emission from

DOI: 10.1021/acs.est.8b04865
Environ. Sci. Technol. 2019, 53, 651−660

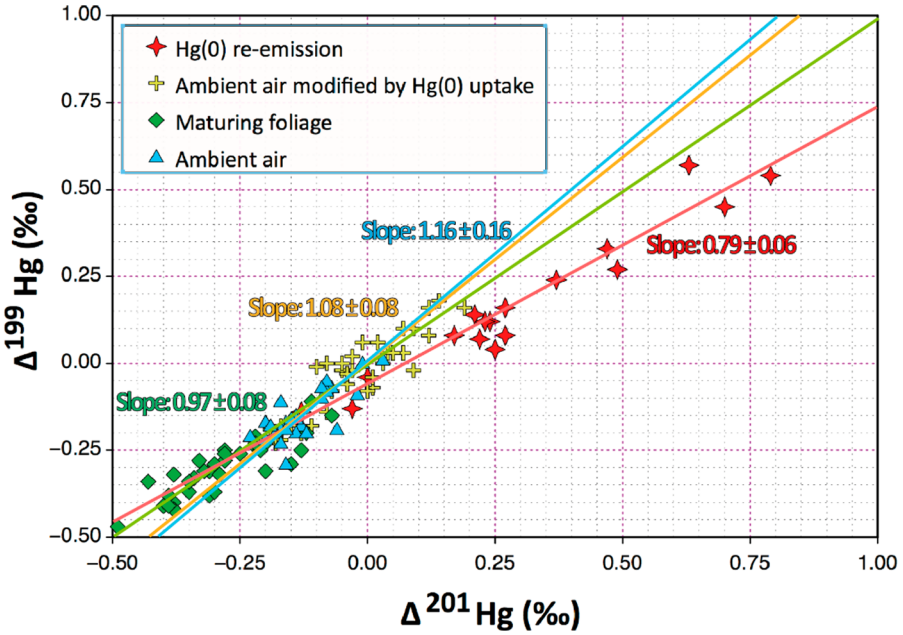

Figure 4. Mass-independent fractionation of odd isotopes (Δ^{199}Hg vs Δ^{201}Hg) of Hg^0 in ambient air (blue filled triangles), in ambient air modified by foliar uptake (yellow filled crosses), Hg^0 re-emissions (red filled stars), and Hg^{II} in maturing foliage (green filled diamonds). Linear fits are obtained from Williamson-York bivariate regression method. Each slope is given with one standard error of the mean.

foliage. Second, foliar Hg odd-MIF shows a significant decreasing trend from leave emergence to senescence, suggesting that Hg^0 emitted from leaf interior. This is because Hg^0 re-emission from foliage surface alone cannot explain such a trend, as the bulk of leaf Hg was found in the tissue compartment (90−96%) with lesser amounts in the surface and cuticle compartments.[27] Although the mobilization of the foliar internal Hg^0 pool is accentuated with Hg-free air as the flushing gas, the action of this flux component under ambient conditions confirmed in this study helps explain the trend toward more negative Δ^{199}Hg in maturing foliage. Finally, similar $\delta^{202}Hg^0$ and $\Delta^{199}Hg^0$ values were observed for washed and regular foliage ($p > 0.05$, 2-tailed paired t test). This cannot be solely explained by foliage surface chemistry change due to leaf washing[36,37] and Hg^0 emitted from newly deposited Hg on leaf surfaces because of washing leading to only 30% smaller Hg^0 re-emission from wash foliage surface than regular foliage. It is more plausible that re-emitted Hg^0 was from the leaf interior.

3.3. Mechanism through Specific Diagnostic Ratios of Compartment Odd-MIF. MIE and NVE have been shown to fractionate specific $\Delta^{199}Hg/\Delta^{201}Hg$ ratios in the range of 1.0−1.3 and 1.6 [20, 38], respectively, during reduction of Hg^{II} [46]. The Δ^{199}Hg vs Δ^{201}Hg plot of Figure 4 shows the isotopic identity of investigated forest ecosystem gas exchange components. The ambient air Hg^0 samples fall within a narrow $\Delta^{199}Hg-\Delta^{201}Hg$ space ($-0.3 < \Delta^{*}Hg < 0.0$‰) and display a $\Delta^{199}Hg/\Delta^{201}Hg$ slope from a Williamson-York regression of 1.16 ± 0.17 ($n = 27$) that aligns within uncertainties to that of a previous study of isotope composition of Hg^0 in ambient air of rural China.[19] In turn, Hg^0 from air-foliage exchange fractionates along a similar slope (1.08 ± 0.08, $n = 36$). In contrast, maturing foliage samples progress along a slope of 0.97 ± 0.08 ($n = 34$) on which also the identity of leaf sprouts overlays. The slope and negative shift in MIF (~−0.25‰) during this progression may serve as an indicator of the reduction pathway as it is characteristic of the reaction mechanism. The photoreduced Hg^0 pool coupled to the measured unidirectional Hg^0 flux data (foliar re-emission from Hg-free air experiments) displays complementary positive ΔHg-values. However, it intriguingly exhibits a slope of 0.79 ± 0.06 ($n = 18$), divergent from that of foliage. Since a slope of $\Delta^{199}Hg/\Delta^{201}Hg \ll 1$ lacks the characteristics of any known elementary processes, the result may be considered as a net MIF combining various MIF effects in multiple pathways with MIE being the dominant process.

Leaves are regarded as thin and well-mixed water pools.[47] Nevertheless, the equilibration of in vivo oxidized Hg^{II} with dominant Hg-binding groups of leaf tissue[16] may cause discernible MDF- and MIF-shifts between the tissue-bound Hg^{II} and Hg^{II} in dissolved aqueous phase.[48] Our observations prompt that the photoreduction yields a net (−)MIE in the foliar Hg^{II} pool in contrast to, e.g., natural waters,[49,50] inferring that the key ligands of Hg^{II} in this system are −SH/−SR groups that form strong Hg−S bonds (log $K_s > 20$).[51] Photoreduction of Hg^{II} bound with extracellular thiol species, such as cysteine, glutathione, and methionine, fractionates with a $\Delta^{199}Hg/\Delta^{201}Hg$-ratio of ~1.2.[45] Another pathway potentially causing Hg-MIF in foliage is abiotic dark reduction by dissolved organic matter.[52] Its odd-isotope enrichment factor [$\varepsilon^{199}_{\text{product/reactant}} = -0.19$ [46]] is smaller but of opposite sign to that of photoreduction [$\varepsilon^{199}_{\text{product/reactant}} = 0.69$],[46] making it isotopically traceable. However, no such evidence can be found in our data. In addition, if abiotic dark reduction dark reduced Hg^{II} would make up a considerable fraction of daily foliar Hg^0 re-emission, then the impact of NVE-driven MIF should shift the observed $\Delta^{199}Hg/\Delta^{201}Hg$-ratio toward 1.6.

Zheng et al.[52] demonstrated that MDF shifts are typically associated with NVE. However, we found that the δ^{202}Hg in the efflux gas under Hg-free gas supply is comparable to signals in foliage ($p = 0.69$, by 2-tailed independent samples test). The observed δ^{202}Hg changes in foliage cannot be solely attributed to the NVE process. As discussed previously, several causes can lead to the change of δ^{202}Hg in foliage. The δ^{202}Hg in foliage

DOI: 10.1021/acs.est.8b04865
Environ. Sci. Technol. 2019, 53, 651−660

can be influenced by the atmospheric Hg^0 assimilation rate in foliage, and dilution by large Hg reservoir in foliage. Specifically, atmospheric Hg^0 uptake by mature foliage can induce (+) 1−2% shift in $\delta^{202}Hg$ of efflux Hg^0, thus largely offset the (−) MDF caused by Hg^0 re-emission.

To quantitatively understand the accumulation of Hg in foliage through atmospheric Hg uptake followed by re-emission, a differential mass accumulation model estimating the progression of foliar MDF and odd-MIF was developed. The formulation and solution of the model are detailed in Section S4 of the SI. The model results were compared to the observations of time-resolved evolution of Hg isotopic composition for SN, LX, and CW. The combined measurements of Hg concentration and isotopic composition in ambient air and Hg^0 flux components collectively suggest that at any time the air−leaf Hg^0 gas exchange is bidirectional as shown in Figure S13 that both uptake and emission occurred progressively over time, although foliar Hg^0 re-emission gains incrementally Hg mass during day-time following insolation. Both Hg uptake and re-emission increase with the foliage growth. The model results suggest that the average of annual re-emitted Hg^0 accounts for 29% of Hg^0 gross uptake by CW foliage, 26% for SN, and 42% for LX, respectively. It should be noted that a mixing model still has significant uncertainties (Figure S14). On the basis of the variability of the observed data from the selected values for the isotopic endmembers, we estimated that the uncertainty to be in the range of 25% to 83% (mean: 56%). The sources of uncertainty are primarily contributed from variable leaf mass and specific leaf area in a given forest ecosystem.

4. IMPLICATIONS

This study presents for the first-time direct evidence for perpetual foliar Hg^0 re-emission that directionally counteracts on foliar Hg^0 uptake and that carries an isotopic signature of (−) MDF and (+) odd-MIF distinguishable from those of the gas-exchange end members foliage and atmospheric Hg^0. Our observations contradict the notion that Hg assimilated in the leaf interior (tissue) becomes withdrawn from current Hg^0 interfacial gas exchange. Instead, the leaf metabolized Hg during the growing season is stored as Hg^{II} and becomes partially recycled to air by interior photoreduction and subsequent evasion. The isotopic signature of ambient air where foliar Hg^0 uptake occurs is complementary to the trend of $\delta^{202}Hg-\Delta^{199}Hg$ space of maturing foliage. Results from an isotopic differential mass balance model infers that the proportion of foliar Hg^0 efflux to uptake gradually increase from emergence to senescence with an average flux ratio over 30%.

Previous studies have suggested that foliage has a potential application as a passive biomonitor of atmospheric Hg.[15,53,54] However, our study clearly demonstrates that foliar Hg content and its isotopic composition are dynamically shaped by bidirectional flux components influenced by the foliage age, species, and insolation level among other parameters. Caution is therefore warranted when using biomass as a proxy in assessing atmospheric Hg input to terrestrial ecosystems. Furthermore, results by global Hg models[38] using isotopic fraction show discrepancies between the predicted odd-MIF in atmospheric Hg^0 (substantially negative since oceanic photoreduction is considered the primary MIF inducing process) and actual observations (near-zero values). Given the measured (+) odd-MIF in foliar re-emission and the massive scale of vegetation over the continents, it is conceivable that this atmospheric source of (+) odd-MIF caused by re-emission can make up for the model-estimated budget inconsistency. Moreover, if the similar degree of reemission occurred throughout global forest ecosystems, the actual gross of Hg^0 by foliage would be greater than the sequestered Hg through litterfall (1000−1200 Mg).[2,3] More measurements are needed to confirm whether the re-emission behavior is consistent at global forest sites.

■ ASSOCIATED CONTENT

Supporting Information

The Supporting Information is available free of charge on the ACS Publications website at DOI: 10.1021/acs.est.8b04865.

The data set of all samples isotopic compositions and fluxes, methodology about detailed field measurements and Hg isotopic mass balance modeling, figures (Figures S1−S15), and tables (Tables S1−S11) (PDF)

■ AUTHOR INFORMATION

Corresponding Authors

*Phone: +86-015885096925; e-mail: jonas@vip.skleg.cn (J.S.).
*Phone: +86-851-85895728; fax: +86-851-5891609; e-mail: fengxinbin@vip.skleg.cn (X.F.).

ORCID

Xun Wang: 0000-0002-7407-8965
Xinbin Feng: 0000-0002-7462-8998

Notes

The authors declare no competing financial interest.

■ ACKNOWLEDGMENTS

This work was funded by the National Natural Science Foundation of China (Grants # 41430754, 41473121, and 41703134), and Opening Fund of the State Key Laboratory of Environmental Geochemistry (SKLEG2017906).

■ REFERENCES

(1) Schroeder, W. H.; Munthe, J. Atmospheric mercury - An overview. *Atmos. Environ.* **1998**, *32* (5), 809−822.
(2) Wang, X.; Bao, Z.; Lin, C.-J.; Yuan, W.; Feng, X. Assessment of Global Mercury Deposition through Litterfall. *Environ. Sci. Technol.* **2016**, *50* (16), 8548−8557.
(3) Obrist, D. Atmospheric mercury pollution due to losses of terrestrial carbon pools? *Biogeochemistry* **2007**, *85* (2), 119−123.
(4) Zhu, W.; Lin, C. J.; Wang, X.; Sommar, J.; Fu, X. W.; Feng, X. B. Global observations and modeling of atmosphere-surface exchange of elemental mercury: a critical review. *Atmos. Chem. Phys.* **2016**, *16* (7), 4451−4480.
(5) Agnan, Y.; Le Dantec, T.; Moore, C. W.; Edwards, G. C.; Obrist, D. New Constraints on Terrestrial Surface Atmosphere Fluxes of Gaseous Elemental Mercury Using a Global Database. *Environ. Sci. Technol.* **2016**, *50* (2), 507−524.
(6) Graydon, J. A.; St Louis, V. L.; Lindberg, S. E.; Hintelmann, H.; Krabbenhoft, D. P. Investigation of mercury exchange between forest canopy vegetation and the atmosphere using a new dynamic chamber. *Environ. Sci. Technol.* **2006**, *40* (15), 4680−4688.
(7) Zhang, H. H.; Poissant, L.; Xu, X. H.; Pilote, M. Explorative and innovative dynamic flux bag method development and testing for mercury air-vegetation gas exchange fluxes. *Atmos. Environ.* **2005**, *39*, 7481−7493.
(8) Fu, X.; Zhu, W.; Zhang, H.; Sommar, J.; Yu, B.; Yang, X.; Wang, X.; Lin, C. J.; Feng, X. Depletion of atmospheric gaseous elemental mercury by plant uptake at Mt. Changbai, Northeast China. *Atmos. Chem. Phys.* **2016**, *16* (20), 12861−12873.

DOI: 10.1021/acs.est.8b04865
Environ. Sci. Technol. 2019, 53, 651−660

(9) Poissant, L.; Pilote, M.; Yumvihoze, E.; Lean, D. Mercury concentrations and foliage/atmosphere fluxes in a maple forest ecosystem in Quebec, Canada. *J. Geophys. Res.* **2008**, *113*, (D10). DOI: 10.1029/2007JD009510.
(10) Luo, Y.; Duan, L.; Driscoll, C. T.; Xu, G. Y.; Shao, M. S.; Taylor, M.; Wang, S. X.; Hao, J. M. Foliage/atmosphere exchange of mercury in a subtropical coniferous forest in south China. *J. Geophys. Res.: Biogeosci.* **2016**, *121* (7), 2006−2016.
(11) Blum, J. D.; Bergquist, B. A. Reporting of variations in the natural isotopic composition of mercury. *Anal. Bioanal. Chem.* **2007**, *388* (2), 353−359.
(12) Enrico, M.; Le Roux, G.; Marusczak, N.; Heimburger, L. E.; Claustres, A.; Fu, X. W.; Sun, R. Y.; Sonke, J. E. Atmospheric Mercury Transfer to Peat Bogs Dominated by Gaseous Elemental Mercury Dry Deposition. *Environ. Sci. Technol.* **2016**, *50* (5), 2405−2412.
(13) Obrist, D.; Agnan, Y.; Jiskra, M.; Olson, C. L.; Colegrove, D. P.; Hueber, J.; Moore, C. W.; Sonke, J. E.; Helmig, D. Tundra uptake of atmospheric elemental mercury drives Arctic mercury pollution. *Nature* **2017**, *547* (7662), 201−204.
(14) Jiskra, M.; Wiederhold, J. G.; Skyllberg, U.; Kronberg, R. M.; Hajdas, I.; Kretzschmar, R. Mercury Deposition and Re-emission Pathways in Boreal Forest Soils Investigated with Hg Isotope Signatures. *Environ. Sci. Technol.* **2015**, *49* (12), 7188−7196.
(15) Wang, X.; Luo, J.; Yin, R. S.; Yuan, W.; Lin, C. J.; Sommar, J.; Feng, X. B.; Wang, H. M.; Lin, C. Using Mercury Isotopes To Understand Mercury Accumulation in the Montane Forest Floor of the Eastern Tibetan Plateau. *Environ. Sci. Technol.* **2017**, *51* (2), 801−809.
(16) Demers, J. D.; Blum, J. D.; Zak, D. R. Mercury isotopes in a forested ecosystem: Implications for air-surface exchange dynamics and the global mercury cycle. *Global Biogeochem Cy* **2013**, *27* (1), 222−238.
(17) Zheng, W.; Obrist, D.; Weis, D.; Bergquist, B. A. Mercury isotope compositions across North American forests. *Global Biogeochem Cy* **2016**, *30* (10), 1475−1492.
(18) Yin, R.; Feng, X.; Meng, B. Stable Mercury Isotope Variation in Rice Plants (Oryza sativa L.) from the Wanshan Mercury Mining District, SW China. *Environ. Sci. Technol.* **2013**, *47* (5), 2238−2245.
(19) Yu, B.; Fu, X. W.; Yin, R. S.; Zhang, H.; Wang, X.; Lin, C. J.; Wu, C. S.; Zhang, Y. P.; He, N. N.; Fu, P. Q.; Wang, Z. F.; Shang, L. H.; Sommar, J.; Sonke, J. E.; Maurice, L.; Guinot, B.; Feng, X. B. Isotopic Composition of Atmospheric Mercury in China: New Evidence for Sources and Transformation Processes in Air and in Vegetation. *Environ. Sci. Technol.* **2016**, *50* (17), 9262−9269.
(20) Blum, J. D.; Sherman, L. S.; Johnson, M. W. Mercury Isotopes in Earth and Environmental Sciences. *Annu. Rev. Earth Planet. Sci.* **2014**, *42*, 249−269.
(21) Sommar, J.; Zhu, W.; Lin, C. J.; Feng, X. Field approaches to measure Hg exchange between natural surfaces and the atmosphere - A review. *Crit. Rev. Environ. Sci. Technol.* **2013**, *43* (15), 1657−1739.
(22) Eckley, C. S.; Gustin, M.; Lin, C. J.; Li, X.; Miller, M. B. The influence of dynamic chamber design and operating parameters on calculated surface-to-air mercury fluxes. *Atmos. Environ.* **2010**, *44* (2), 194−203.
(23) Fu, X.; Heimbuerger, L.-E.; Sonke, J. E. Collection of atmospheric gaseous mercury for stable isotope analysis using iodine- and chlorine-impregnated activated carbon traps. *J. Anal. At. Spectrom.* **2014**, *29* (5), 841−852.
(24) Zhou, J.; Feng, X.; Liu, H.; Zhang, H.; Fu, X.; Bao, Z.; Wang, X.; Zhang, Y. Examination of total mercury inputs by precipitation and litterfall in a remote upland forest of Southwestern China. *Atmos. Environ.* **2013**, *81*, 364−372.
(25) Sun, R. Y.; Enrico, M.; Heimburger, L. E.; Scott, C.; Sonke, J. E. A double-stage tube furnace-acid-trapping protocol for the pre-concentration of mercury from solid samples for isotopic analysis. *Anal. Bioanal. Chem.* **2013**, *405* (21), 6771−6781.
(26) Bash, J. O.; Bresnahan, P.; Miller, D. R. Dynamic surface interface exchanges of mercury: A review and compartmentalized modeling framework. *Journal of Applied Meteorology and Climatology* **2007**, *46*, 1606−1618.
(27) Laacouri, A.; Nater, E. A.; Kolka, R. K. Distribution and uptake dynamics of mercury in leaves of common deciduous tree species in Minnesota, U.S.A. *Environ. Sci. Technol.* **2013**, *47* (18), 10462−10470.
(28) Osterwalder, S.; Fritsche, J.; Alewell, C.; Schmutz, M.; Nilsson, M. B.; Jocher, G.; Sommar, J.; Rinne, J.; Bishop, K. A dual-inlet, single detector relaxed eddy accumulation system for long-term measurement of mercury flux. *Atmos. Meas. Tech.* **2016**, *9*, 509−524.
(29) Sommar, J.; Zhu, W.; Shang, L.; Lin, C. J.; Feng, X. Seasonal variations in metallic mercury (Hg0) vapor exchange over biannual wheat−corn rotation cropland in the North China Plain. *Biogeosciences* **2016**, *13* (7), 2029−2049.
(30) Converse, A. D.; Riscassi, A. L.; Scanlon, T. M. Seasonal variability in gaseous mercury fluxes measured in a high-elevation meadow. *Atmos. Environ.* **2010**, *44* (18), 2176−2185.
(31) Bash, J. O.; Miller, D. R. Growing season total gaseous mercury (TGM) flux measurements over an Acer rubrum L. stand. *Atmos. Environ.* **2009**, *43* (37), 5953−5961.
(32) Yu, Q.; Luo, Y.; Wang, S.; Wang, Z.; Hao, J.; Duan, L. Gaseous elemental mercury (GEM) fluxes over canopy of two typical subtropical forests in south China. *Atmos. Chem. Phys.* **2018**, *18* (1), 495−509.
(33) Millhollen, A. G.; Gustin, M. S.; Obrist, D. Foliar mercury accumulation and exchange for three tree species. *Environ. Sci. Technol.* **2006**, *40* (19), 6001−6006.
(34) Stamenkovic, J.; Gustin, M. S. Nonstomatal versus Stomatal Uptake of Atmospheric Mercury. *Environ. Sci. Technol.* **2009**, *43* (5), 1367−1372.
(35) Rutter, A. P.; Schauer, J. J.; Shafer, M. M.; Creswell, J. E.; Olson, M. R.; Robinson, M.; Collins, R. M.; Parman, A. M.; Katzman, T. L.; Mallek, J. L. Dry deposition of gaseous elemental mercury to plants and soils using mercury stable isotopes in a controlled environment. *Atmos. Environ.* **2011**, *45* (4), 848−855.
(36) Oliva, S. R.; Raitio, H. Review of cleaning techniques and their effects on the chemical composition of foliar samples. *Boreal Environ. Res.* **2003**, *8* (3), 263−272.
(37) Rea, A. W.; Lindberg, S. E.; Keeler, G. J. Assessment of dry deposition and foliar leaching of mercury and selected trace elements based on washed foliar and surrogate surfaces. *Environ. Sci. Technol.* **2000**, *34* (12), 2418−2425.
(38) Sonke, J. E. A global model of mass independent mercury stable isotope fractionation. *Geochim. Cosmochim. Acta* **2011**, *75* (16), 4577−4590.
(39) Sun, G.; Sommar, J.; Feng, X.; Lin, C.-J.; Ge, M.; Wang, W.; Yin, R.; Fu, X.; Shang, L. Mass-Dependent and -Independent Fractionation of Mercury Isotope during Gas-Phase Oxidation of Elemental Mercury Vapor by Atomic Cl and Br. *Environ. Sci. Technol.* **2016**, *50* (17), 9232−41.
(40) Chen, J. B.; Hintelmann, H.; Feng, X. B.; Dimock, B. Unusual fractionation of both odd and even mercury isotopes in precipitation from Peterborough, ON, Canada. *Geochim. Cosmochim. Acta* **2012**, *90*, 33−46.
(41) Donovan, P. M.; Blum, J. D.; Yee, D.; Gehrke, G. E.; Singer, M. B. An isotopic record of mercury in San Francisco Bay sediment. *Chem. Geol.* **2013**, *349*, 87−98.
(42) Gratz, L. E.; Keeler, G. J.; Blum, J. D.; Sherman, L. S. Isotopic Composition and Fractionation of Mercury in Great Lakes Precipitation and Ambient Air. *Environ. Sci. Technol.* **2010**, *44* (20), 7764−7770.
(43) Buchachenko, A. L. Magnetic isotope effect: Nuclear spin control of chemical reactions. *J. Phys. Chem. A* **2001**, *105* (44), 9995−10011.
(44) Bigeleisen, J. Nuclear size and shape effects in chemical reactions. Isotope chemistry of the heavy elements. *J. Am. Chem. Soc.* **1996**, *118*, 3676−3680.
(45) Zheng, W.; Hintelmann, H. Isotope Fractionation of Mercury during Its Photochemical Reduction by Low-Molecular-Weight Organic Compounds. *J. Phys. Chem. A* **2010**, *114* (12), 4246−4253.

(46) Hintelmann, H.; Zheng, W. Tracking Geochemical Transformations and Transport of Mercury through Isotope Fractionation. In *Environmental Chemistry and Toxicology of Mercury*; Liu, G., Cai, Y., O'Driscoll, N., Eds.; John Wiley & Sons: Hoboken, 2011; pp 293–328.
(47) Yakir, D.; Sternberg, L. D. L. The use of stable isotopes to study ecosystem gas exchange. *Oecologia* **2000**, *123* (3), 297–311.
(48) Wiederhold, J. G.; Cramer, C. J.; Daniel, K.; Infante, I.; Bourdon, B.; Kretzschmar, R. Equilibrium Mercury Isotope Fractionation between Dissolved Hg(II) Species and Thiol-Bound Hg. *Environ. Sci. Technol.* **2010**, *44* (11), 4191–4197.
(49) Bergquist, B. A.; Blum, J. D. Mass-dependent and -independent fractionation of Hg isotopes by photoreduction in aquatic systems. *Science* **2007**, *318*, 417–420.
(50) Zheng, W.; Hintelmann, H. Mercury isotope fractionation during photoreduction in natural water is controlled by its Hg/DOC ratio. *Geochim. Cosmochim. Acta* **2009**, *73* (22), 6704–6715.
(51) Gerbig, C.; Ryan, J.; Aiken, G., The Effects of Dissolved Organic Matter on Mercury Biogeochemistry. In *Environmental Chemistry and Toxicology of Mercury*; Liu, G., Cai, Y., O'Driscoll, N., Eds.; John Wiley & Sons: Hoboken, NJ, 2011; pp 259–292.
(52) Zheng, W.; Hintelmann, H. Nuclear Field Shift Effect in Isotope Fractionation of Mercury during Abiotic Reduction in the Absence of Light. *J. Phys. Chem. A* **2010**, *114* (12), 4238–4245.
(53) Huang, J.; Lyman, S. N.; Hartman, J. S.; Gustin, M. S. A review of passive sampling systems for ambient air mercury measurements. *Environmental Sciences: Processes and Impacts* **2014**, *16* (3), 374–392.
(54) Gustin, M. S.; Amos, H. M.; Huang, J.; Miller, M. B.; Heidecorn, K. Measuring and modeling mercury in the atmosphere: A critical review. *Atmos. Chem. Phys.* **2015**, *15*, 5697–5713.

DOI: 10.1021/acs.est.8b04865
Environ. Sci. Technol. 2019, 53, 651–660